

Article

The Role of Hydrogen in Hydrogen Embrittlement of Metals: The Case of Stainless Steel

Young Suk Kim ^{1,*}, Sung Soo Kim ¹ and Byung Hak Choe ²

¹ Korea Atomic Energy Research Institute; Daejeon 34057, Korea; sskim6@kaeri.re.kr

² Department of Advanced Metals & Materials Engineering, Gangneung-Wonju National University, Gangneung 25457, Korea; cbh@gwnu.ac.kr

* Correspondence: yskim1@kaeri.re.kr; Tel.: +82-42-868-2359

Received: 1 February 2019; Accepted: 28 March 2019; Published: 3 April 2019



Abstract: Hydrogen embrittlement (HE) of metals has remained a mystery in materials science for more than a century. To try to clarify this mystery, tensile tests were conducted at room temperature (RT) on a 316 stainless steel (SS) in air and hydrogen of 70 MPa. With an aim to directly observe the effect of hydrogen on ordering of 316 SS during deformation, electron diffraction patterns and images were obtained from thin foils made by a focused ion beam from the fracture surfaces of the tensile specimens. To prove lattice contraction by ordering, a 40% CW 316 SS specimen was thermally aged at 400 °C to incur ordering and its lattice contraction by ordering was determined using neutron diffraction by measuring its lattice parameters before and after aging. We demonstrate that atomic ordering is promoted by hydrogen, leading to formation of short-range order and a high number of planar dislocations in the 316 SS, and causing its anisotropic lattice contraction. Hence, hydrogen embrittlement of metals is controlled by hydrogen-enhanced ordering during RT deformation in hydrogen. Hydrogen-enhanced ordering will cause the ordered metals to be more resistant to HE than the disordered ones, which is evidenced by the previous observations where furnace-cooled metals with order are more resistant to HE than water-quenched or cold worked metals with disorder. This finding strongly supports our proposal that strain-induced martensite is a disordered phase.

Keywords: hydrogen embrittlement; stainless steel; ordering; planar dislocations; furnace cooled; water quenched

1. Introduction

Since the 19th century, it has been widely accepted that hydrogen embrittlement (HE) occurs in metals. Many studies have been conducted to identify its mechanism which remains unknown to date. Two of the most commonly invoked mechanisms for metals with no formation of hydrides are hydrogen-enhanced decohesion (HEDE) and hydrogen-enhanced localized plasticity (HELP) [1]. The former suggests that hydrogen reduces the atomic cohesive strength, leading to brittle fracture whereas the latter proposes hydrogen-enhanced mobility of dislocations and dislocation slip localization. However, it remains to be clarified how a decrease in the atomic cohesive strength by hydrogen can occur and how hydrogen-enhanced mobility of dislocations can lead to slip localization, enhanced crack growth and finally intergranular (IG) cracking.

Recently, we observed that strain-induced martensite (SIM) formed during tensile tests underwent lattice expansion in hydrogen-free 304 stainless steel (SS) but lattice contraction in hydrogen-charged 304 SS [2], and that SIM formation was suppressed by hydrogen, leading to hydrogen embrittlement. As a result, we have proposed that SIM is a disordered phase created by the destruction of short-range ordered DO₃-(Fe, Cr)₃Ni and that hydrogen promotes ordering in 304 SS, leading to suppression of SIM formation, the latter of which was enhanced with decreasing strain rate. Note that hydrogen-enhanced

ordering has already been observed at high temperatures in Alloy 600 [3], Pd₃Mn [4], CoPt thin films [5], pure Ni [6] and Fe [7]. However, direct evidence for the enhanced formation of the ordered phase by hydrogen during deformation even at room temperature has been lacking. The aim of this study is to experimentally demonstrate that hydrogen-enhanced ordering occurs in metals during room temperature (RT) deformation under a high-pressure hydrogen gas, and that HE of metals is controlled by the degree of ordering occurring during deformation in hydrogen.

2. Materials and Methods

Tensile specimens were taken from a 316 SS that was water quenched after solution annealing. Its chemical composition was 18Cr-10Ni-2Mo-Fe (in weight percent) [8]. Tensile tests were conducted in air or hydrogen of 70 MPa at a strain rate of 10⁻³/s and RT. Note that tensile specimens were exposed to hydrogen of 70 MPa for 300 min prior to tensile tests [8] and high pressure hydrogen gas was used to give rise to ordering during RT deformation even at a high strain rate of 10⁻³/s. To directly observe formation of the ordered phase at fracture surfaces, electron diffraction patterns and images were obtained using a transmission electron microscope (TEM) (JEOL, JEOL 2000FX, Tokyo, Japan) from thin foils that were made by a focused ion beam from the fracture surfaces of the tensile specimens. Electron diffraction patterns were taken along the zone axes, such as [111], [110], and [112] to show a short-range order (SRO) formed during RT tensile tests. To check if SIM formation was suppressed by hydrogen during the tensile tests, the hardness and amount of SIM at and near the fracture surfaces of the 316 SS were determined, respectively, using a ferritoscope (Helmut Fisher Korea Co, Feritcope-MP30, Korea) and a Vickers hardness tester (Shimadzu, HMV 2000, Kyoto, Japan). The detailed procedure to determine the amount of SIM has been reported elsewhere [2]. Vickers hardness measurements were performed using a Shimadzu hardness tester (HMV 2000, Kyoto, Japan), according to ASTM E92-82 [9]. The Vickers hardness in HV was averaged from over six measurements. The fracture surfaces of the specimens after RT tensile tests were also examined by scanning electron microscopy (SEM) (JEOL, S-4000, Japan). To show the effect of ordering on lattice contraction, a neutron diffraction analysis was conducted using a neutron diffractometer (KAERI, Republic of Korea) installed in the Hanaro at the Korea Atomic Energy Research Institute. The instrumental resolution of the diffractometer was $\Delta d/d \cong 0.04\%$. The change in peak position (peak shift) was used to determine a change in lattice parameter and its sensitivity was less than 1/10th of the instrumental resolution.

3. Results

Figure 1 shows the fracture shapes of 316 SS after tensile tests in air and 70 MPa H₂. Ductile cup and cone fracture and brittle flat fracture were observed in air and hydrogen, respectively. With the fracture surfaces (Figure 1) examined at a high magnification, ductile dimples with multiple shallow craters were clearly observed in air, as shown in Figure 2, whereas quasi-cleavage fracture appeared in hydrogen. Figures 1 and 2 show that HE occurred in the 316 SS during deformation at RT in hydrogen. To relate the HE of the 316 SS to hydrogen-suppressed formation of SIM as already observed in a 304 SS, the amount of SIM formed in the 316 SS was determined from the fractured surfaces. As shown in Table 1, the amount of SIM was 43 vol.% in air, but it decreased considerably to 15 vol.% in hydrogen. Given that hydrogen-suppressed formation of SIM has been observed in a 304 SS irrespective of the magnitude of tensile strain [2], a reduced amount of SIM in the 316 SS when tested in hydrogen is related primarily to the hydrogen effect. The reduction of SIM by hydrogen decreased the hardness of 316 SS to 345 HV when compared to that when tested in air (393 HV) (Table 1). This result agrees perfectly with our previous observations [2], revealing that hydrogen suppresses SIM formation in austenitic stainless steels.

To provide direct evidence for hydrogen-enhanced ordering even at RT, electron diffractions and images were obtained using TEM thin foils which were acquired using a focused ion beam directly from the fracture surfaces shown in Figure 2. Figure 3 shows TEM images of the fracture surfaces of 316 SS deformed in hydrogen and air, respectively [8]. Irrespective of the environment, planar

dislocations were observed at the fracture surface, but their number was higher in hydrogen than in air. The results of Figure 3 agree perfectly with the observations of Nibur [10] and Robertson [11] that hydrogen increased the number of slip steps or enhanced slip planarity, respectively. The electron diffraction patterns of the images in Figure 3 are shown in Figure 4 [8]. The bright $1/3 \{422\}$ and $1/2 \{311\}$ reflections, both of which are normally forbidden in a face-centered cubic lattice, were observed in hydrogen (Figure 4a,b), along the $[111]$ and $[112]$ zone axes, respectively. In contrast, in air, the $1/3 \{422\}$ forbidden reflections were very diffuse (red circles added for a guidance) and the $1/2 \{311\}$ reflections were hardly observed (Figure 4c,d, respectively).

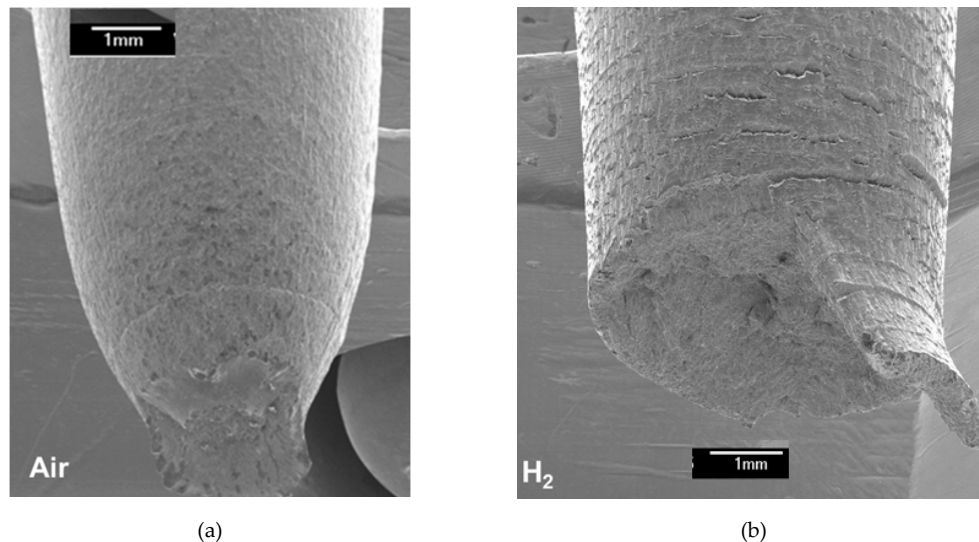


Figure 1. (a) Cup and cone fracture and (b) flat fracture of a 316 SS when tested in air and 70 MPa of hydrogen, respectively.

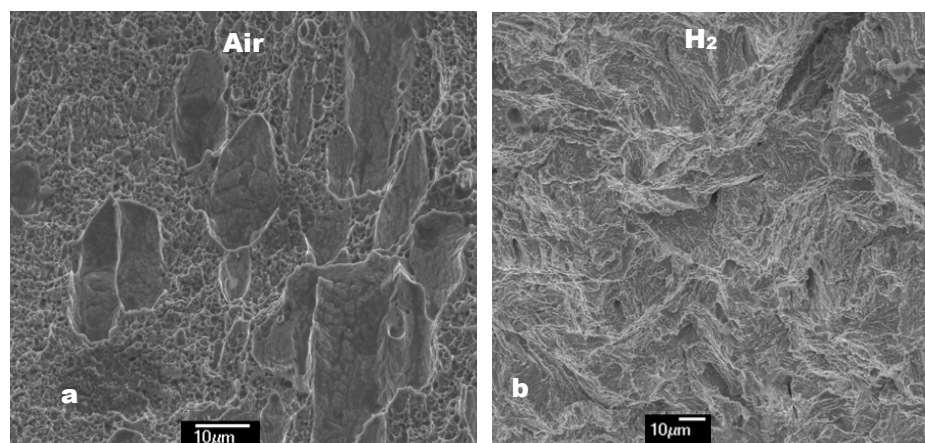


Figure 2. (a) Ductile dimple fracture and (b) quasi-cleavage fracture of a 316 SS when tested in air and hydrogen, respectively.

Table 1. Amount of SIM (vol.%) and hardness (HV) determined at or near the fracture surfaces of a 316 SS after RT tensile deformation in air and hydrogen.

Parameters	Testing Conditions	
	Air	H ₂
Amount of strain-induced martensite (SIM) (%)	43 ± 4	15 ± 4
Hardness (HV)	393 ± 15	345 ± 15

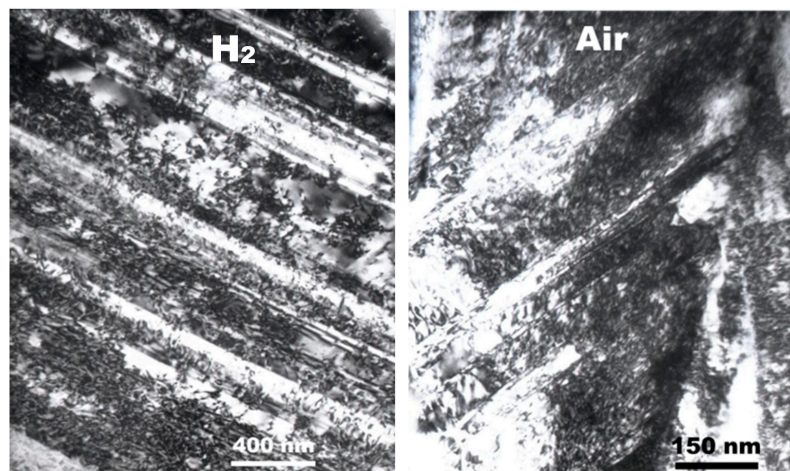


Figure 3. Planar dislocations formed at the fracture surfaces of a 316 SS after tensile tests in hydrogen and air, respectively (reproduced from [8] with permission from BH Choe, 2019).

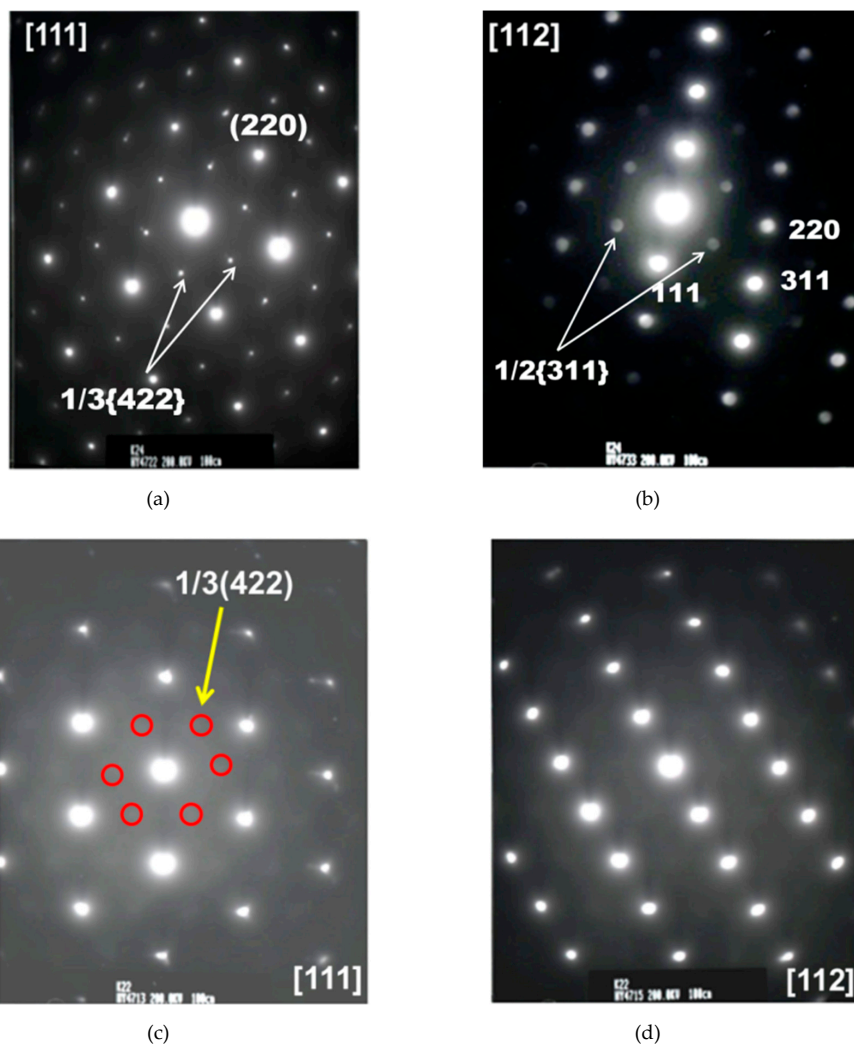


Figure 4. Diffraction patterns taken along the [111] and [112] zone axes of a 316 SS after tensile tests in (a,b) hydrogen and (c,d) air, respectively (adapted from [8] with permission from BH Choe, 2019).

When viewed along the [110] zone axis, these forbidden reflections disappeared; however, twinning spots appeared instead in hydrogen and air, as shown in Figure 5. As shown in Figure 5a,c, twinning streaks were observed to align along a direction perpendicular to the planar dislocation boundaries (Figure 5b,d), likely, due to the twin of a very thin platelet [12]. Note that twinning spots, as shown in Figure 5a,c, are always observed in the [110] zone axis whenever electron diffraction patterns are taken from the planar dislocations as shown in Figure 5b,d. A typical example is diffraction patterns of Alloy 600 after SCC tests in 360 °C water containing dissolved oxygen below 10 ppb, as shown in Figure 6 [3]. Diffuse $1/3 \{422\}$ and $1/2 \{311\}$ reflections were also observed in the [111] and [112] zone axes along with twinning spots appearing in the [110] zone axis. In contrast, with a diffraction pattern taken along the [110] zone axis only but along neither the [111] nor [112] zone axis, the planar dislocations of Figure 3 may be mistaken to correspond to twinning due to twinning spots, as shown in Figure 5a,c and Figure 6c. Thus, the higher number of planar dislocations formed in hydrogen charged metals is often called hydrogen-enhanced twinning [13,14] because of the diffraction pattern taken only along the [110] zone axis.

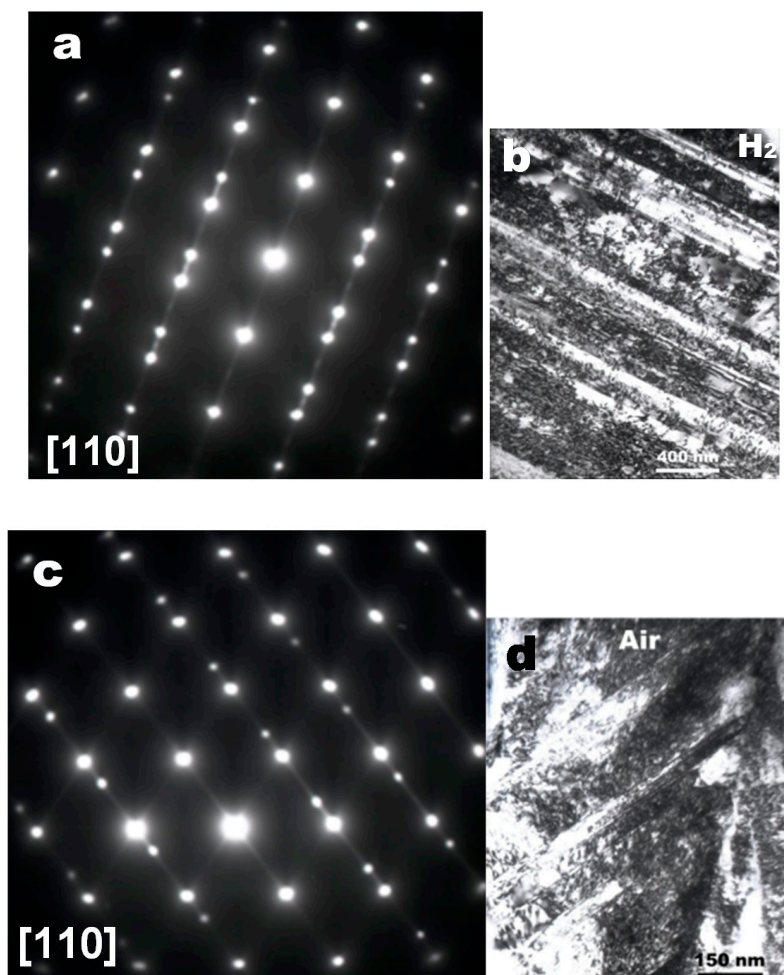


Figure 5. Twinning spots and streaks (a,c) observed when the planar dislocations (b,d) formed on the fracture surfaces of a 316 SS deformed in hydrogen (a,b) and air (c,d), respectively, were examined in the [110] zone axis. (b,d) added intentionally to show the twin streaks aligned perpendicular to planar dislocation boundaries (reproduced from [8] with permission from BH Choe, 2019).

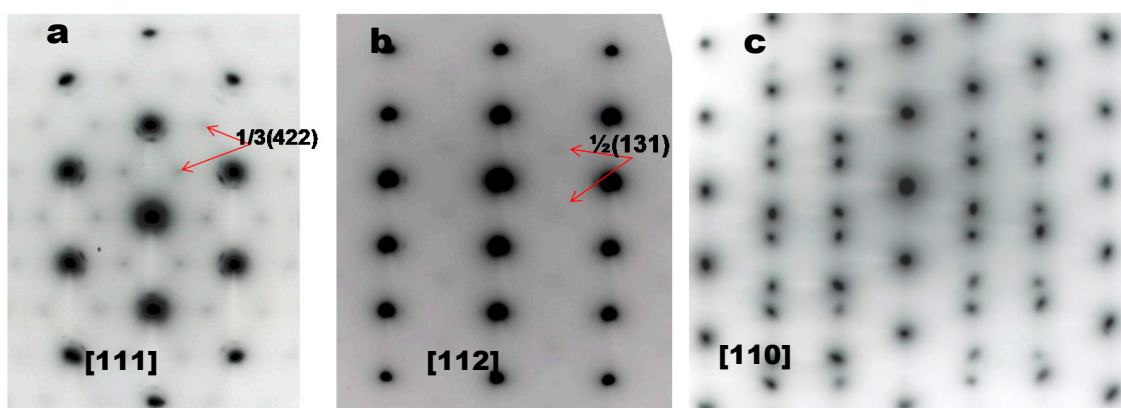


Figure 6. Diffraction patterns taken along the [111], [112] and [110] zone axes of Alloy 600 after stress corrosion cracking tests in 360 °C water (reproduced from [3] with permission from YS Kim, 2019).

To show the effect of ordering on the magnitude of lattice parameter change, a 316 SS was cold worked to 40% and aged at 400 °C for up to approximately 20,000 h. Its chemical composition was 16.7Cr-10.2Ni-2.0Mo-1.1Mn-0.03N-0.02C-Fe (bal.) in wt.%. Its lattice parameters were determined by neutron diffraction analysis before and after aging at 400 °C. Upon aging at 400 °C, as shown in Figure 7, lattice contractions were observed in 40% CW 316 SS by ordering, the magnitude of which differed with grain orientation or plane. Here, the lattice contraction is termed a fractional change of d-spacing of the lattice planes after aging over that before aging. The {200} planes showed the highest lattice contraction of 0.07% when compared to the other planes, indicating anisotropic lattice contraction with grain orientation. Note that anisotropic lattice contraction has been observed also in Alloy 600 with the {111} planes exhibiting the highest lattice contraction [15].

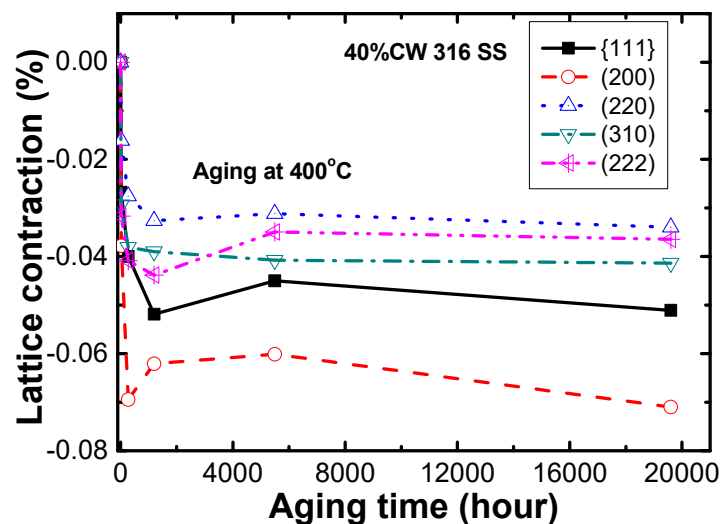


Figure 7. Lattice contractions of 40% cold worked 316 SS upon aging at 400 °C.

4. Discussion

4.1. Formation of Short-Range Order in 316 SS Due to Hydrogen-Enhanced Ordering

As shown in Figure 4, the bright $1/3$ {422} and $1/2$ {311} forbidden reflections were observed in deformed 316 SS in high-pressure hydrogen of 70 MPa but not in air, revealing short-range order (SRO) formed during RT deformation because of hydrogen. Although the diffuse $1/3$ {422} forbidden reflections had been observed in 310 SS cathodically charged with hydrogen during deformation at RT [16], the bright $1/3$ {422} reflections as shown in Figure 4 seem to be first observed. Moreover,

the same $1/3$ {422} forbidden reflections were noted in aged metals [17,18], $\text{Hg}_3\text{In}_2\text{Te}_6$ crystals grown by the Bridgeman method [19], an austenitic Fe-Mn-Al alloy after tensile deformation at 77 K [20] and in Alloy 600 after stress corrosion cracking (SCC) tests in 360 °C water [3]. The bright $1/3$ {422} reflections as shown in Figure 4a appeared in the last three cases (i.e., $\text{Hg}_3\text{In}_2\text{Te}_6$ crystals grown by the Bridgeman method [19], an austenitic Fe-Mn-Al alloy after tensile deformation at 77 K [20] and in Alloy 600 after SCC tests in 360 °C water [3]). Moreover, when the [111] diffraction pattern was tilted around the [110] axis until the [112] was obtained, the bright $1/2$ {311} reflections were observed as shown in Figure 4b, which had also been observed in aged metals [18,21] and $\text{Hg}_3\text{In}_2\text{Te}_6$ crystals [19]. By observing that the lattice spacing of the $1/3$ {422} forbidden reflections determined by electron diffraction was around 0.21 nm for Alloy 600, which agreed perfectly with that determined by neutron diffraction, we have already confirmed that the $1/3$ {422} and $1/2$ {311} forbidden reflections formed in Alloy 600 correspond to SRO. Interestingly, the lattice spacing of the $1/3$ {422} forbidden reflections for 316 SS deformed in hydrogen, as shown in Figure 4a, was also determined to be approximately 0.21 nm, which is found to be the same as that for Ni charged with hydrogen [22]. Hence, the $1/3$ {422} and $1/2$ {311} forbidden reflections observed in the 316 SS deformed in hydrogen (Figure 4a,b) must correspond to SRO, but not to anything else [8,16,23,24]. Furthermore, as the intensity of the forbidden reflections of the 316 SS was much stronger in hydrogen than in air, as shown in Figure 4, it is evident that hydrogen promoted SRO formation. In short, we demonstrate that hydrogen promoted ordering in 316 SS even during RT deformation, leading to SRO formation, which has never been considered in the HE mechanisms proposed so far. Specifically, during deformation even at RT in hydrogen, ordering occurred to some degree in the 316 SS, which was significantly suppressed without hydrogen as shown in Figure 4. In fact, although hydrogen-enhanced ordering had already been observed at high temperatures in metals [3–7], ordering can hardly occur at RT where diffusion of atoms is too slow unless ordering is enhanced by hydrogen. Consequently, the occurrence of hydrogen-enhanced ordering at RT in 316 SS is very surprising. Supportive evidence for hydrogen-enhanced ordering is Kimura's observations [22] that, firstly, a new phase was formed before the (111) plane, according to X-ray diffraction analysis, and, secondly, IG cracking occurred in a 20 μm nickel sheet with hydrogen charged at a current density of 100 A/m^2 for 1 h and then aged at RT for 24 h. His observations reveal that hydrogen caused formation of an additional phase or SRO and, moreover, IG cracking even without applied stresses. Given our previous observations [3] that IG cracking of Alloy 600 occurred primarily due to ordering (or short-range ordering), leading to lattice contraction, the IG cracking of pure nickel after hydrogen charging is related entirely to hydrogen-enhanced ordering. Another example of hydrogen-enhanced ordering is that the yield stress of a 310 SS cathodically charged with 5.8% of hydrogen increased to around twice that of a hydrogen-free 310 SS [16]. Supportive evidence for SRO formation by hydrogen-enhanced ordering is the presence of the planar dislocations shown in Figure 3, according to [25] revealing that the existence of SRO was the primary cause of planar slip. The higher number of planar dislocations formed in hydrogen (Figure 3) suggests that a higher degree of SRO was formed in the 316 SS when tested in hydrogen, as confirmed in Figure 4, reducing the volume of martensite corresponding to the disordered phase, as shown in Table 1, or hydrogen-suppressed formation of SIM.

Our recent observations were that strain-induced martensite (SIM) formed during tensile tests underwent lattice expansion in hydrogen-free 304 stainless steel (SS) but lattice contraction in hydrogen-charged 304 SS [2] and that its formation was suppressed by hydrogen, leading to hydrogen embrittlement. As a result, we have proposed that SIM is a disordered phase created by the destruction of short-range ordered $\text{DO}_3\text{-(Fe, Cr)}_3\text{Ni}$ and hydrogen promotes ordering in 304 SS, leading to suppression of SIM formation. In fact, indirect evidence that SIM is a disordered phase has been provided by an increase in tensile elongation with increasing volume of SIM for hydrogen-free 304 SS because disorder improves ductility [3,26]. Direct evidence for our rationale, however, is first provided by the observations of the $1/3$ {422} and $1/2$ {311} forbidden reflections in 316 SS during RT deformation in hydrogen, as shown in Figure 4. Furthermore, considering that hydrogen-suppressed formation

of SIM occurred in 316 SS during RT deformation in high-pressure hydrogen, as shown in Table 1, it is evident that hydrogen whether it is cathodically charged or hydrogen gas restraints formation of SIM in austenitic SS. As SIM is a disordered phase, hydrogen-suppressed formation corresponds to hydrogen-enhanced ordering whose solid evidence is lattice contraction of SIM in hydrogen-charged 304 SS during deformation at RT [2].

4.2. Effect of Hydrogen-Enhanced Ordering

As with solidification shrinkage occurring during the phase transition from the disordered liquid to the ordered solid, ordering generates internal compressive stresses within the matrix of grains which are anisotropic, causing anisotropic lattice contractions, as shown in Figure 7. The generation of internal compressive stresses within grains induces tensile stresses localized in the vicinity of boundaries including grain and twin boundaries to counteract them. Due to anisotropic lattice contractions, as shown in Figure 7, the localized tensile stresses at grain boundaries are also anisotropic or change with the lattice plane of grains or grain orientation, as schematically shown in Figure 8. In other words, the magnitude of tensile stresses locally produced at grain boundaries is anisotropic, which is graphically expressed as the length of the arrows, as shown in Figure 8. When the localized tensile stresses at grain boundaries generated by ordering exceed the grain boundary strength, then IG cracking occurs [3,27,28]. If the formers are not large enough to exceed the latter, then, voids can take place at a grain boundary, for example, between grains A and B, as shown in Figure 8, leading to brittle transgranular fracture as described in Figures 1b and 2b. Compelling evidence for IG cracking by ordering is provided by the observations of Kohara [29] and Kim [3] that IG cracking occurred in CuAu by an ordering reaction even without applied stresses, and furnace cooled (FC-) Ni₃Fe with SRO showed IG cracking during RT deformation in air, respectively. The generation of localized tensile stresses in the vicinity of grain boundaries is corroborated by the observations of higher strains [30,31], higher dislocation density [32] or higher hardness [33] in their vicinity than in the matrix. Note that the generation of localized tensile stresses by hydrogen-enhanced ordering has never been recognized in any of the HE mechanisms proposed so far.

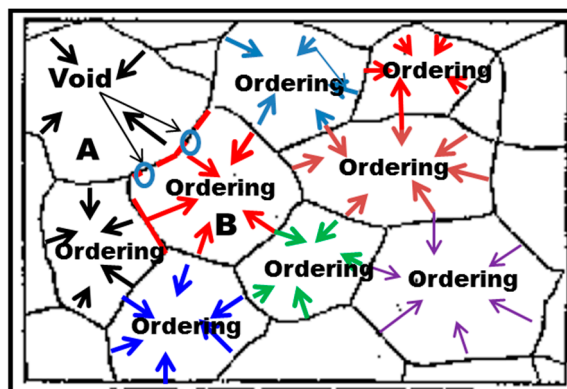


Figure 8. Diagram showing the spontaneous generation of localized tensile stresses in the vicinity of grain boundaries by ordering leading to lattice contraction. Note that voids are formed on the grain boundary between grains A and B when the localized tensile stress at a grain boundary between the two grains is lower than the grain boundary strength.

Hence, the role of hydrogen is not to decrease the cohesive strength of atoms as suggested by the HEDE mechanism but to promote ordering, leading to a decrease in the lattice spacing of atoms in metals, spontaneously inducing the development of tensile stresses localized in the vicinity of grain boundaries. The localized tensile stresses spontaneously generated at grain boundaries are the driving force causing IG cracking and/or brittle transgranular fracture, the significance of which has never been fully appreciated to date. Consequently, the susceptibility to HE of metals

depends on the degree of ordering occurring during deformation in hydrogen: the higher the degree of hydrogen-enhanced ordering, the higher the susceptibility to HE of metals. Furthermore, the compressive stresses generated in the lattice by hydrogen-enhanced ordering are the driving force for immobile dislocations existing in the lattice to be forced to move upon exposure to hydrogen [11]. Thus, hydrogen-enhanced ordering can account for two of the mostly invoked mechanisms such as HEDE and HELP. In short, hydrogen-enhanced ordering is the cause of HE of metals.

FC-Alloy 600 with SRO showed a higher resistance to SCC than water-quenched (WQ-) one with disorder, which is related to the degree of ordering (or short-range ordering) occurring during SCC tests [3,27,28]. Likewise, since the HE of metals is controlled also by hydrogen-enhanced ordering, it is expected that FC-metals with a higher level of order would be more resistant to HE than WQ-metals with either a lower level of order or disorder. Note that order herein represents SRO, but not long-range order (LRO). This is because, during deformation in hydrogen, those with a higher level of order due to furnace-cooling will have a lower lattice contraction due to a low degree of ordering, generating lower localized tensile stresses, which leads to higher resistance to HE. In contrast, those with disorder due to water quenching will experience a higher lattice contraction due to a high degree of ordering, generating high tensile stresses, which leads to lower resistance to HE. Compelling evidence is indeed provided by Okada's observations [34] that FC-Fe-20Cr-22Ni showed no loss of fracture strain upon RT deformation after cathodic charging of hydrogen and a very slight decrease in fracture strain even during in-situ hydrogen charging conditions. Marquez [35] also showed that FC-Fe-10Ni-C had a higher resistance to HE than WQ-metal. Baek [36] has recently shown that a 304L SS made by laser-aided direct metal tooling (DMT) has a higher resistance to HE than a cold rolled (CR) one when deformed in 10 MPa pressurized hydrogen gas. Then, he claimed that the manufacturing process affected the sensitivity of a steel to HE but did not pinpoint which process had this effect and why. Considering that the yield stress of the DMT specimen was 1.7 times as high as that of the CR specimen, it seems that the DMT specimen underwent slow cooling during DMT, resulting in SRO formation and thus an increase in yield stress. Supportive evidence is the larger grains (several hundreds of micrometers) of the DMT specimen when compared to the small grains (29 μm) of the CR specimen, indicating that it experienced slow cooling, leading to fast grain growth. In other words, the DMT specimen had SRO to some degree whereas the CR specimen had disorder due to cold rolling. When deformed in hydrogen, it seems that hydrogen-enhanced ordering occurred little in the DMT specimen with SRO, but significantly in the CR specimen with disorder. In other words, little occurrence of hydrogen-enhanced ordering in the former with SRO led to little loss of its tensile elongation in hydrogen when compared to that in air, but its significant occurrence in the latter with disorder led to low resistance to HE. Thus, Baek's results [36] agree with the observations of Okada [34] and Marquez [35] in that the ordered metals obtained by furnace-cooling were more resistant to HE than the disordered ones obtained by water quenching or cold working. Consequently, the HE of metals is controlled by the degree of ordering occurring during RT deformation in hydrogen or after hydrogen charging.

By contrast, Han [37] and Briant [38], respectively, showed that WQ-austenitic stainless steels (or called solution annealed ones) were more resistant to HE than sensitized ones like FC-ones. Note that hydrogen gas pressure applied by them was 1 MPa when compared to 70 MPa used in this study so that hydrogen-enhanced ordering seems difficult to occur during RT deformation. In this case, WQ-ones with disorder were more resistant to HE than sensitized or FC-ones with SRO, which is opposite to the observations of [34–36]. Considering no occurrence of hydrogen-enhanced ordering during deformation in very low-pressure hydrogen gas, higher resistance to HE of WQ-metals with disorder than FC-metals with SRO is related to the own characteristics of disorder and SRO, respectively: disorder and SRO are ductile and brittle, respectively. Supportive evidence is our previous observations [3] that WQ-Ni₃Fe with disorder and FC-one with SRO showed ductile and IG brittle fracture, respectively, during RT deformation, even without hydrogen. So, depending on experimental conditions such as hydrogen pressure or hydrogen charging conditions, hydrogen-enhanced ordering

can or cannot occur during RT deformation. Considering that hydrogen enhanced ordering occurs in structural materials which will deform at a very slow strain rate in high-pressure hydrogen gas, however, the results obtained in conditions without hydrogen-enhanced ordering seem to be worthless from the engineering viewpoint.

Some researchers [39–41] have claimed that the HE of metals is controlled by hydrogen diffusion so that martensite serving as a fast diffusion path for hydrogen is detrimental to the HE of austenitic stainless steels. However, despite hydrogen diffusion being much faster in FC-metals (i.e., X-65 and F 22 alloys) than WQ-metals [42], the former showed a higher resistance to HE than the latter according to the previous observations [34–36]. In other words, FC-metals with a higher hydrogen diffusion coefficient were found to have a higher resistance to HE. This finding reveals that HE is not related to hydrogen diffusion, which is contrary to the claims made in the previous studies [39–41]. Note that it has been confirmed only in bcc metals. Considering the occurrence of hydrogen-enhanced ordering not only in fcc metals but also in bcc metals, however, this finding is also valid in the formers. Consequently, the HE of metals is controlled not by hydrogen diffusion but by hydrogen-enhanced ordering.

5. Conclusions

With tensile deformation conducted on a 316 SS in hydrogen and air, hydrogen suppressed formation of SIM. Using electron diffraction patterns taken along the [111], [112] and [110] zone axes from the 316 SS deformed in air and hydrogen, we demonstrate that atomic ordering was promoted by hydrogen, leading to SRO formation manifested as the bright $1/3 \{422\}$ and $1/2 \{311\}$ forbidden reflections and a high number of planar dislocations. The ordering caused anisotropic lattice contractions with grain orientation for a 316 SS, spontaneously generating localized tensile stresses primarily in the vicinity of grain boundaries, which are the driving force for brittle transgranular fracture or IG cracking of metals. In short, the resistance to HE of metals is controlled by the degree of hydrogen-enhanced ordering occurring during deformation in hydrogen. Strong evidence is provided in the literature where FC-metals are more resistant to HE, due to a low degree of ordering, when compared to WQ- or cold worked metals. This finding strongly supports our proposal that SIM is a disordered phase.

Author Contributions: Conceptualization, Y.S.K.; Investigation, B.H.C., S.S.K., Y.S.K.; Data Curation, S.S.K., Y.S.K.; Writing, Y.S.K.; Writing—Review & Editing, Y.S.K.; Supervision, Y.S.K.

Funding: This research was funded by the National Research Foundation of Korea (NRF) grant funded by the Korean government (the Korean Ministry of Science and ICT) [No. NRF-2017M2A8A4017282].

Acknowledgments: Special thanks are due to S.S. Lee who conducted the neutron diffraction experiment at KAERI and to J.Y. Jung for his support for this work.

Conflicts of Interest: The authors declare no conflict of interest. The founding sponsors had no role in the design of the study; in the collection, analyses, or interpretation of data; in the writing of the manuscript, and in the decision to publish the results.

References

1. Gerberich, W.W.; Stauffer, D.D.; Sofronis, P. A coexistent view of hydrogen effects on mechanical behavior of crystals: HELP and HEDE. In *Effects of Hydrogen on Materials, Proceedings of the 2008 International Hydrogen Conference, Moran, WY, USA, 7–10 September 2008*; Somerday, B., Sofronis, P., Jones, R., Eds.; ASM International: Materials Park, OH, USA; pp. 38–45.
2. Kim, Y.S.; Bak, S.H.; Kim, S.S. Effect of strain-induced martensite on tensile properties and hydrogen embrittlement of 304 stainless steel. *Metall. Mater. Trans. A* **2016**, *47A*, 222–230. [[CrossRef](#)]
3. Kim, Y.S.; Maeng, W.Y.; Kim, S.S. Effect of short-range ordering on stress corrosion cracking susceptibility of Alloy 600 studied by electron and neutron diffraction. *Acta Mater.* **2015**, *83*, 507–515. [[CrossRef](#)]
4. Flanagan, T.B.; Craft, A.P.; Kuji, T.; Baba, K.; Sakamoto, Y. Hydrogen induced disorder-order transition in Pd₃Mn. *Scr. Metall.* **1986**, *20*, 1745–1750. [[CrossRef](#)]

5. Yang, F.; Wang, H.; Wang, H.; Zhang, J.; Zhu, J. Effect of hydrogen annealing on L1₀ ordering transformation and magnetic properties of CoPt thin films on B₄C underlayer. *J. Phys. D Appl. Phys.* **2009**, *42*, 115001. [[CrossRef](#)]
6. Fukai, Y.; Shizuku, Y.; Kurokawa, Y. Superabundant vacancy formation in Ni-H alloys. *J. Alloys Compd.* **2001**, *329*, 195–201. [[CrossRef](#)]
7. Horoi, T.; Fukai, Y.; Mori, K. The phase diagram and superabundant vacancy formation in Fe-H alloys revisited. *J. Alloys Compd.* **2005**, *404–406*, 252–255. [[CrossRef](#)]
8. Baek, U.B.; Choe, B.H.; Shim, J.H.; Kim, Y.U.; Kim, Y.S.; Kim, S.S.; Nam, S.H.; Hong, K. Hydrogen induced crack and phase transformation in hydrogen pressured tensile test of 316L stainless steel. *Korean J. Met. Mater.* **2015**, *53*, 82–89.
9. ASTM International. *ASTM E92-82, Standard Test Methods for Vickers Hardness of Metallic Materials*; ASTM International: West Conshohocken, PA, USA, 1997.
10. Nibur, K.A.; Bahr, D.F.; Somerday, B.P. Hydrogen effects on dislocation activity in austenitic stainless steel. *Acta Mater.* **2006**, *54*, 2677–2684. [[CrossRef](#)]
11. Robertson, I.M. The effect of hydrogen on dislocation dynamics. *Eng. Fract. Mech.* **1999**, *64*, 649–673. [[CrossRef](#)]
12. Farrel, K.; Byun, T.S.; Hashimoto, N. Deformation mode maps for tensile deformation of neutron-irradiated structural alloys. *J. Nucl. Mater.* **2004**, *335*, 471–486. [[CrossRef](#)]
13. Astafurova, E.G.; Zakharova, G.G.; Maier, H.J. Hydrogen-induced twinning in <001> Hadfield steel single crystals. *Scr. Mater.* **2010**, *63*, 1189–1192. [[CrossRef](#)]
14. Rigsbee, J.M.; Benson, R.B. A TEM investigation of hydrogen-induced deformation twinning and associated martensite phases in 304-type stainless steel. *J. Mater. Sci.* **1977**, *12*, 406–409. [[CrossRef](#)]
15. Kim, S.S.; Kim, D.W.; Kim, Y.S. Lattice contraction behavior of atomic ordering in Alloy 600. *Korean J. Met. Mater.* **2014**, *52*, 963–968. [[CrossRef](#)]
16. Abraham, D.P.; Altstetter, C.J. Hydrogen-enhanced localization of plasticity in an austenitic stainless steel. *Metall. Mater. Trans. A* **1995**, *26A*, 2859–2871. [[CrossRef](#)]
17. Marucco, A.; Nath, B.J. Effects of ordering on the properties of Ni-Cr alloys. *J. Mater. Sci.* **1988**, *23*, 2107–2114. [[CrossRef](#)]
18. Jiang, X.J.; Noble, B.; Waterloo, G.; Tafto, J. Differential scanning calorimetry and electron diffraction investigation on low-temperature aging in Al-Zn-Mg alloys. *Metall. Mater. Trans. A* **2000**, *31A*, 339–348. [[CrossRef](#)]
19. Luo, L.; Jie, W.; Xu, Y.; He, Y.; Xu, L.; Fu, L. HRTEM study of the ordered phases in Hg₃In₂Te₆ crystals grown by Bridgman method. *R. Soc. Chem.* **2014**, *16*, 5073–5079. [[CrossRef](#)]
20. Sato, K.; Ichinose, M.; Hitotsu, Y.; Inoue, Y. Effects of deformation induced transformation and twinning on the mechanical properties of austenitic Fe-Mn-Al alloys. *ISIJ Int.* **1989**, *29*, 868–877. [[CrossRef](#)]
21. Marucco, A. Atomic ordering in the Ni-Cr-Fe system. *Mater. Sci. Eng. A* **1994**, *189*, 267–276. [[CrossRef](#)]
22. Kimura, A.; Birnbaum, H.K. The effects of cathodically charged hydrogen on the flow stress of nickel and nickel-carbon alloys. *Acta Metall.* **1987**, *35*, 1077–1088. [[CrossRef](#)]
23. Pashley, D.W.; Stowell, M.J. Electron microscopy and diffraction of twinned structures in evaporated films of gold. *Philos. Mag. A* **1963**, *8*, 1605–1632. [[CrossRef](#)]
24. Cherns, D. Direct resolution of surface atomic steps by transmission electron microscopy. *Philos. Mag. A* **1974**, *30*, 549–556. [[CrossRef](#)]
25. Gerold, V.; Karnthaler, H.P. On the origin of planar slip in F.C.C. alloys. *Acta Metall.* **1989**, *37*, 2177–2183. [[CrossRef](#)]
26. Baker, I.; Munroe, P.R. Improving intermetallic ductility and toughness. *JOM* **1988**, *40*, 28–31. [[CrossRef](#)]
27. Kim, Y.S.; Kim, S.S.; Kim, D.W. Intergranular stress corrosion cracking (IGSCC) of Alloy 600 with cooling rate. In Proceedings of the 16th International Symposium on Environmental Degradation of Materials in Nuclear Power Systems-Water Reactors, Asheville, NC, USA, 11–15 August 2013.
28. Kim, Y.S.; Kim, S.S. Origins of negative strain rate dependence of stress corrosion cracking initiation in Alloy 690, and intergranular crack formation in thermally treated Alloy 690. *Metall. Mater. Trans. A* **2016**, *47A*, 4353–4356. [[CrossRef](#)]
29. Kohara, S.; Kuzynski, G.C. Internal stresses during ordering. *Acta Metall.* **1956**, *2*, 221–222. [[CrossRef](#)]

30. Ehrnsten, U.; Saukkonen, T.; Karlsen, W.; Hanninen, H. Deformation localization and EAC in inhomogeneous microstructures of austenitic stainless steels. In Proceedings of the 14th International Symposium on Environmental Degradation of Materials in Nuclear Power Systems-Water Reactors, Virginia Beach, VA, USA, 23–27 August 2009; pp. 910–919.
31. Kim, S.W.; Hwang, S.S.; Lee, J.M. Effect of local strain distribution on stress corrosion cracking of cold rolled Alloy 690 with inhomogeneous microstructure. *Corrosion* **2015**, *71*, 1071–1081. [[CrossRef](#)]
32. Park, K.T.; Kim, Y.S.; Lee, J.G.; Shin, D.H. Thermal stability and mechanical properties of ultrafine grained low carbon steel. *Mater. Sci. Eng. A* **2000**, *293*, 165–172. [[CrossRef](#)]
33. Floreen, S.; Westbrook, J.H. Grain boundary segregation and the grain size dependence of strength of nickel-sulfur alloys. *Acta Metall.* **1969**, *17*, 1175–1181. [[CrossRef](#)]
34. Okada, H.; Hosoi, Y.; Abe, S. Formation of cracks in austenitic stainless steels cathodically charged with hydrogen. *Corrosion* **1970**, *26*, 183–186. [[CrossRef](#)]
35. Marquez, J.A.; Matsushima, I.; Uhlig, H.H. Effect of cold rolling on resistance of Ni-Fe alloys to hydrogen cracking. *Corrosion* **1970**, *26*, 315–322. [[CrossRef](#)]
36. Baek, S.W.; Song, E.J.; Kim, J.H.; Jung, M.; Baek, U.B.; Nahm, S.H. Hydrogen embrittlement of 3-D printing manufactured austenitic stainless steel part for hydrogen service. *Scr. Mater.* **2017**, *130*, 87–90. [[CrossRef](#)]
37. Han, G.; He, J.; Fukuyama, S.; Yokogawa, K. Effect of strain-induced martensite on hydrogen environment embrittlement on sensitized austenitic stainless steels at low temperatures. *Acta Mater.* **1998**, *46*, 4559–4570. [[CrossRef](#)]
38. Briant, C.L. Hydrogen assisted cracking of sensitized 304 stainless steel. *Metall. Trans. A* **1978**, *9A*, 731–733. [[CrossRef](#)]
39. Zhang, L.; Wen, M.; Imade, M.; Fukuyama, S.; Yokogawa, K. Effect of nickel equivalent on hydrogen gas embrittlement of austenitic stainless steels based on type 316 at low temperatures. *Acta Mater.* **2008**, *56*, 3414–3421. [[CrossRef](#)]
40. Mine, Y.; Narazaki, C.; Murakami, K.; Matsuoka, S.; Murakami, Y. Hydrogen transport in solution-treated and pre-strained austenitic stainless steels and its role in hydrogen-enhanced fatigue crack growth. *Int. J. Hydrogen Energy* **2009**, *34*, 1097–1107. [[CrossRef](#)]
41. Papula, S.; Talonen, J.; Todoshchenko, O.; Hanninen, H. Effect of internal hydrogen on delayed hydride cracking of metastable low-nickel austenitic stainless steels. *Metall. Mater. A* **2014**, *45A*, 5270–5279. [[CrossRef](#)]
42. Fallahmohammadi, E.; Bolzoni, F.; Fumagalli, G.; Re, G.; Benassi, G.; Lazzari, L. Hydrogen diffusion into three metallurgical microstructures of a C-Mn X65 and low alloy F22 sour service steel pipelines. *Int. J. Hydrogen Energy* **2014**, *39*, 13300–13313. [[CrossRef](#)]



© 2019 by the authors. Licensee MDPI, Basel, Switzerland. This article is an open access article distributed under the terms and conditions of the Creative Commons Attribution (CC BY) license (<http://creativecommons.org/licenses/by/4.0/>).